Spectrochimica Acta Part A: Molecular and Biomolecular Spectroscopy 302 (2023) 122953

Contents lists available at ScienceDirect

Spectrochimica Acta Part A:
Molecular and Biomolecular Spectroscopy

journal homepage: www.journals.elsevier.com/spectrochimica-acta-part-a-molecular-and-biomolecular-spectroscopy

A rapid colorimetric method for the detection of carminic acid in samples based on visible color change

Azra Akbar [a], Amna Jabbar Siddiqui [b], Syed Tarique Moin [d], Muhammad Noman Khan [a], Ali Raza [a], Adeeba Khadim [a], Muhammad Usman [a], M. Iqbal Choudhary [a,b,c,d], Syed Ghulam Musharraf [a,b,c,*]

[a] H.E.J. Research Institute of Chemistry, International Center for Chemical and Biological Sciences, University of Karachi, Karachi 75270, Pakistan
[b] Dr. Panjwani Center for Molecular Medicine and Drug Research, International Center for Chemical and Biological Sciences, University of Karachi, Karachi 75270, Pakistan
[c] Halal Certification, Testing and Research Services (HCTRS), H.E.J. Research Institute of Chemistry, International Center for Chemical and Biological Sciences, University of Karachi, Karachi 75270, Pakistan
[d] Third World Center for Science and Technology, H.E.J. Research Institute of Chemistry, International Center for Chemical and Biological Sciences, University of Karachi, Karachi 75270, Pakistan

HIGHLIGHTS

- A cost-effective method based on the detection of carminic acid using lead nitrate.
- A rapid color change is observed which can be easily differentiated from the human eye.
- Carminic acid can be detected with a LOD of 0.0025 mg mL^{-1}.
- Applicable to the wide use of samples including food and the non-food items.
- The structural study of Carminic acid-Pb^{2+} complexes was also studied.

GRAPHICAL ABSTRACT

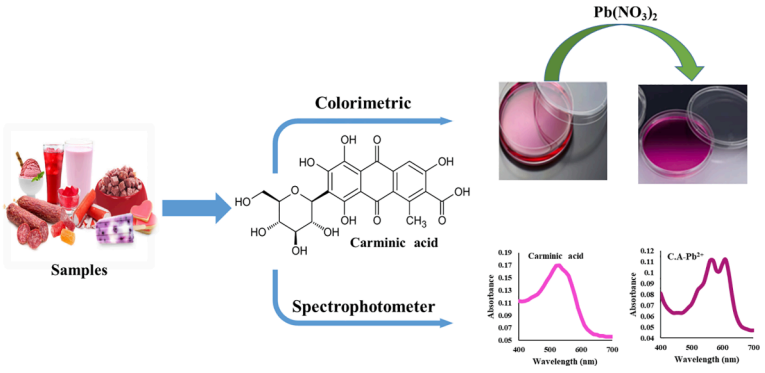

ARTICLE INFO

Keywords:
CA
Food Dyes
Insect-based
CA-Fe^{2+} Complex Inhibition

ABSTRACT

Carminic Acid (CA), an insect-derived red color, is widely used as a colorant and additive in food and non-food items. The detection of CA is of great concern since it is unacceptable for vegetarians and vegans consumers. Therefore, it is important for food authorities to have a rapid detection method for CA. We describe here a simple and rapid method for the qualitative detection of CA, using Pb^{2+} for complex formation. As a result, the sample solution shows a visible change from pink to purple (bathochromic shift) which could also be analyzed through a spectrophotometer at λ_{max} = 605 nm. The structure of the CA-Pb^{2+} complex was also studied through advanced spectroscopic techniques. Moreover, the presence of iron results in the formation of a stable CA-Fe^{2+} complex without any significant color change, as Fe^{2+} has a stronger binding affinity with CA. Thus, sodium fluoride

* Corresponding author at: H.E.J. Research Institute of Chemistry, International Center for Chemical and Biological Sciences, University of Karachi, Karachi 75270, Pakistan.
E-mail address: musharraf@iccs.edu (S. Ghulam Musharraf).

https://doi.org/10.1016/j.saa.2023.122953
Received 17 January 2023; Received in revised form 22 May 2023; Accepted 29 May 2023
Available online 6 June 2023

(NaF) was used to prevent CA-Fe^{2+} complex formation. Therefore, two methods were developed based on the absence (method I) and presence (method II) of NaF. The LOD and LOQ for the method I was 0.0025 and 0.0076 mg mL^{-1}, and for method II, values were 0.0136 and 0.0415 mg mL^{-1}, respectively. The methods were also validated by intra and inter-day analyses. A total of 45 commercials, including food and non-food samples, were screened for the detection of CA. The developed methods are applicable for the effective and rapid surveillance of CA in various samples without the use of high-tech instruments.

1. Introduction

Natural colors are broadly classified as plant, animal, and mineral colors, although plants are the major sources of natural color [1]. CA is an insect-based natural red colorant that can be extracted from the dried bodies of female *Dactylopius coccus* Costa insect species, commonly known as cochineal insects [2–4]. However, the use of color from insects is not allowed or acceptable by people of different faiths and lifestyles. [5]. As the European Union and the United States have restricted the use of synthetic colorants as food additives, the use of natural colorants, such as CA in the food industry has increased substantially. Currently, the main use of CA is in cosmetics, foods, pharmaceuticals, textile, and plastic industries. This dye is allowed in most of the different countries; with a food additive identification code of E-120 [6]. It has been used extensively in place of E122, E124, and E129 food colors. Food safety issues due to various colorants have become very common for example, by adding Sudan red and CA to paprika [7]. CA is routinely added to food products. However, its long-term intake is detrimental to human health as it may cause allergic reactions and even anaphylactic shock [8]. Food safety, therefore, involves strict monitoring such food additives such as CA.

Till now, several methods for the determination of CA in food samples have been developed, including spectrophotometry [9,10], high-performance liquid chromatography [11,12], capillary electrophoresis [13,14], differential pulse polarography [8], and stripping voltammetry [15,16]. In addition to the analytical method, the extraction of the analyte is an important factor to avoid interfering species in food matrices. Several sample preparation methods for the detection of carmine/ CA are reported in the literature, including solid-phase extraction [17–19], liquid–liquid extraction [20], cloud point extraction [21,22], and ultrasonic-assisted extraction [9,23]. The diversity of the chemical classes of natural colors, the complexities of their structures, and the wide range of applications in foods and beverages present analytical challenges that in turn requires efficient and specific analytical procedures. The development of efficient extraction procedures is necessary, especially as many of the natural coloring components are unstable, and require to separation of colors from the samples. Thus there is a continuous need for the development of a rapid, and inexpensive method for the determination of CA in various samples.

We here in reported a simple and rapid method for the detection of CA in both food and non-food samples without using a laborious and time-consuming extraction procedure and expensive instruments. It is based on visible color change using lead nitrate as a complex formation with CA. The above method has been successfully applied for the selective identification of CA. To the best of our knowledge, this is the first report on the identification of CA in food and non-food samples without applying any expensive extraction protocol and instrumental analysis.

2. Materials and methods

2.1. Chemicals and reagents

CA 95.78% was purchased from Sigma–Aldrich (USA). All metal salts and other chemicals (95–98%), such as zinc sulfate, cobalt chloride, strontium chloride, sodium chloride, potassium chloride, nickel sulfate, vanadium sulfate, rhodium, iron sulfate, lead nitrate, magnesium chloride, calcium chloride, copper chloride, tin chloride dehydrate, cadmium sulfate, sodium hydroxide, and hydrochloric acid were purchased from E. Merck (USA). Ultra-pure water was made available using the Direct 16 Milli-Q purification system (Millipore Co., USA). Other 10 red dyes include Ponceau 4R (**1**), Allura red AC (**2**), Carmoisine (**3**), Acid Red 1 (**4**), Amaranth (**5**), Erythrosine B (**6**), Acid Red 14 (**7**), Direct Red 17 (**8**), Ponceau SX (**9**) and Acid Red 92 (**10**) were purchased from Sigma–Aldrich (USA).

2.2. Preparation of standard solution

CA stock solution (2 mg mL^{-1}) was prepared in 10 mM HEPES buffer of pH = 7 and was stored in the dark at a low temperature (4 °C).

2.3. Preparation of calibration curve solutions

For the calibration curve, the stock solution of 2 mg mL^{-1} of CA was diluted to a series of different concentrations (0.492, 0.369, 0.246, 0.147, and 0.073 mg mL^{-1}). Similarly, the Pb^{2+} stock solution of 2 mg mL^{-1} solution was diluted to a series of different Pb^{2+} concentrations (0.207, 0.155, 0.103, 0.062, 0.031 mg mL^{-1}). The same concentrations of CA and Pb^{2+} solutions were added in a mole ratio of 1:2.

2.4. Preparation of metal ions solutions

Stock aqueous solutions of all metal ions (2 mg mL^{-1}) were prepared in de-ionized water. To screen the formation of the complexes of CA with fifteen metals, the CA and metal ions solutions were mixed in a mole ratio of 1:2. The physical color change was observed before analyzing the sample. The solution was shaken properly then the spectrum was recorded on a U.V. visible spectrophotometer at room temperature.

2.5. Preparation of buffer solutions

Different buffer solutions (10 mM) of pH 4.0, 5.1, 6.0, 7.1, 8.0, 9.1, and 10.2 were prepared for the optimum pH experiment. 0.024 mg mL^{-1} CA was prepared in buffer tablets of pH 4, acetate buffer (pH 5), phosphate buffer (pH 6), HEPES buffer (pH 7), tricine buffer (pH 8), borate buffer (pH 9), and ammonia buffer (pH 10). Each buffer solution was mixed with 0.020 mg mL^{-1} Pb^{2+} aqueous solution in a 1:2 ratio for spectrophotometric analysis.

2.6. Preparation of azo-dye solutions

Stock solutions of azo-dyes (2 mg mL^{-1}) were prepared in HEPES buffer. The solutions were sonicated for 1 min and wrapped with aluminum foil to protect them from light. The stock solutions remained stable for approximately six months at a temperature of 4 °C.

2.7. Sample collection and preparation

A total of 45 samples of consumer goods were purchased from local supermarkets. These samples were categorized into three groups, i.e. foods (32), cosmetics (10), and pharmaceuticals (3). The samples were stored at 4 °C until processed for extraction of CA. To detect CA in samples, hydrolysis was performed with HCl to convert carmine into CA. Five gm of each sample was first mixed with 3 mL of HCl (2 M) for solid samples and 2 mL of HCl (2 M) for liquid samples, followed by

homogenization in an ultrasonic bath at room temperature. The homogenized samples were placed in a water bath at 62 °C for 15–20 min. After that, the mixture was cooled, and the solution was centrifuged for 10 min at 5000 rpm. NaF was added to a 4% aliquot of the sample, followed by pH 7 adjusted with 1 M NaOH. The lead paper strip was added to this solution, and the presence of CA was inferred from the color change, from pink to purple.

Spiked samples for method validation were prepared similarly to the samples. The 300 μL of the sample plus an amount of standard solution, corresponding to spike concentrations of 0.135, 0.226, and 0.316 mg mL^{-1}, were diluted to a final volume of 1500 μL for each of three samples and labeled as SA1, SA2, and SA3, respectively.

2.8. Spectrophotometric analysis

All absorption spectra were recorded on a multimode reader spectrophotometer (Synergy HTX Plate Reader-Agilent BioTek country). All samples were analyzed using round-bottom 96-well plates, and absorbance was measured at a wavelength of 300 to 700 nm with increments of 05 nm. The radiation source was a xenon flash lamp.

2.9. Synthesis and analysis of the complex

CA (0.02 mmol) in HEPES buffer 1 mL of pH = 7 was mixed with a drop-wise aqueous solution of $Pb(NO_3)_2$ (0.02 mmol). The reaction mixture was stirred at room temperature for 30 min. The resulting precipitates were centrifuged for 10 min at 12,000 rpm. The supernatant was discarded and the precipitate was air-dried.

Tandem mass spectra of CA and its complex were obtained using Bruker Amazon Speed Ion Trap Mass Spectrometer (Germany) in positive ionization mode. The samples were directly introduced into the ion trap mass spectrometer with a flow rate of 5 μL/ min through a syringe pump. The electrospray voltage was set at 4.0 Kv, and the capillary temperature was set at 200 °C. The mass range was between *m/z* 50 to 2000. Nuclear Magnetic Resonance (NMR) spectra were recorded in DMSO-d_6 as a solvent on Bruker Aspect AM 500 and AM 600 NMR spectrometers (Switzerland). The chemical shifts (δ) are in ppm, and the coupling constant (*J*) is in Hz. Spectra Fourier-transform infrared spectroscopy (FT-IR) were recorded by using a TENSCO II (Bruker, Germany) instrument equipped with an ATR single reflection diamond, in the range of 4000–500 cm^{-1} with 32 scans at a resolution of 4 cm^{-1}.

2.10. Density functional theory calculations

Different metal–ligand complexes were formed between lead ion (Pb^{2+}) and CA (CA) and optimized at the density functional theory (DFT) level using B3LYP functionals and Los Alamos National Laboratory 2 double zeta (LANL2DZ) basis set with effective core potential (ECP) basis set for lead atom. 6-31G (d,p) basis sets were used for non-metals in the gas phase and the continuum solvent [24–27]. All the optimization calculations were performed using Gaussian 0.9 [28]. The strength of metal–ligand complexes was estimated in terms of interaction energy calculated between Pb^{2+} and CA in different metal-to-ligand ratios using the following equation.

$$E_{Int} = E_{AB} - E_A - E_B$$

Where E_{Int} is the interaction energy of any complex between any two molecules ***A*** and ***B*** which is calculated as the energy difference between the complex and the separately calculated energies as E_A and E_B for each components ***A*** and ***B***.

3. Results and discussion

3.1. Screening of different metals with CA

To study the complex formation of CA with fifteen different metals, the metal solutions were mixed with 50 μL of CA in a mole ratio of 1:1, 2:1, and 1:2. The visible color change from pink to purple was observed only upon the mixing of Pb^{2+} with CA. The absorption spectra were recorded at room temperature. The maximum absorbance of CA was at a wavelength of 527 nm, and with a shoulder at 580 nm, as illustrated (Fig. 1A). The absorption spectra revealed a decrease in the absorption at a wavelength of 527 nm, while the band increases at the wavelength of 558 nm. The appearance of a (bathochromic) red-shift band was centered at a wavelength of 605 nm. On the other hand, no other metal ions exhibited significant color differences and spectral changes. However, the addition of Mg^{2+}, Ca^{2+}, Cd^{2+}, Cu^{2+}, and Sn^{2+} showed hypochromic or hyperchromic effects in the absorption spectra, but no significant change in color was observed in these solutions. The color changes after the addition of various metal ions as shown in Fig. 1B. Among these metals, Fe^{2+} forms a complex with CA appeared at λ_{max} = 540 nm, but no significant color change was observed. This indicates that the Pb^{2+} ion changes color due to the formation of the complex can be used for CA determination. Such studies have been reported previously about the chelation of CA with various metal ions to form metal complexes at different pH [9].

3.2. pH studies for the complex of CA with Pb^{2+}

The effect of pH on the complex formation between CA and Pb^{2+} was also studied in an aqueous solution at pH ranges of 4 to 10. In the presence of the two-mole ratio of Pb^{2+} with CA, the absorption band at wavelength 605 was observed in between pH 7 to 9. It exhibited a maximum absorption at pH 7.0, as shown in Fig. 2. Remarkably, no binding interaction between CA and Pb^{2+} was observed at highly basic pH and acidic in conditions. Above pH 10 and below pH 6, no change in color was observed. The formation of the CA-Pb^{2+} complex and color development is significantly influenced by the pH. When the pH is below 7, the CA molecule exists predominantly in its protonated form, which hinders the formation of the CA-Pb^{2+} complex and color change. In contrast, when the pH is at 7, CA is mostly in its deprotonated form, allowing it to bind more effectively with Pb^{2+} ions and formed a color complex. Therefore, pH control is critical in the formation of the CA-

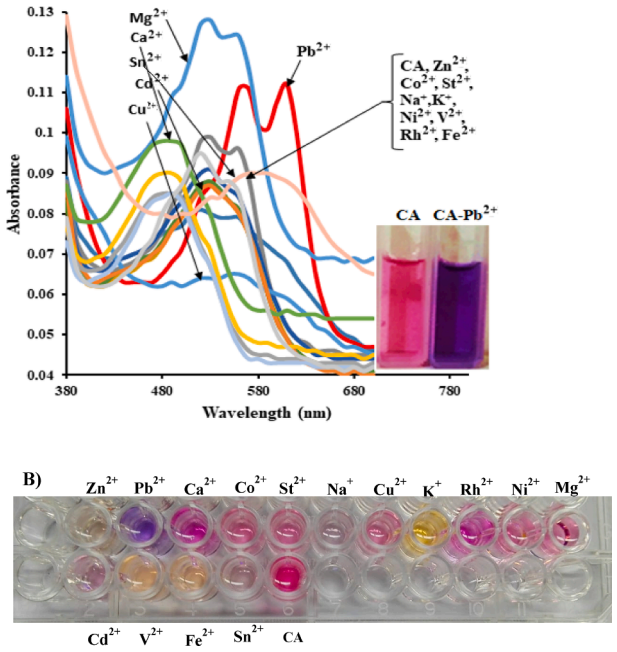

Fig. 1. A) Absorption spectra of CA in the presence of different metal ions in a mole ratio 1:2. Photograph showing the color change of CA (left) and in the presence of Pb^{2+} (right). **B)** Color changes of the CA after the addition of various metal ions in a mole ratio of 1:2.

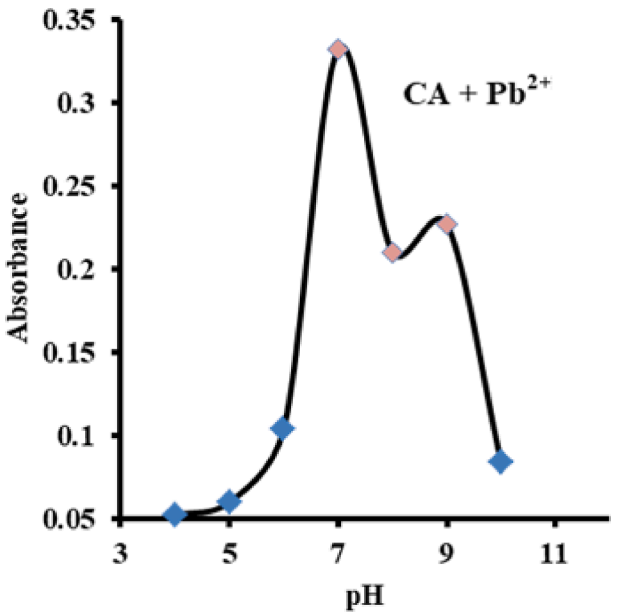

Fig. 2. Absorbance spectrum at 605 nm of CA with Pb^{2+} in a mole ratio of 1:2 at different pH values.

Pb^{2+} complex and color development. In this method, HEPES buffer pH 7.0 was selected. This buffer with an ampholyte zwitter ionic structure provides a comprehensive range of buffering capacity. A HEPES is binding affinity to metal ions is almost negligible. The CA complexation with various metals at different pH is previously reported [11,29]. At pH 5.8, a CA-copper complex is formed [30]. Similarly, gallium also form a stable complex with CA at pH 4.0 [31].

3.3. Effect of other dyes in complex formation

We also studied the effect of the other 10 red dyes using the same method. Each dye was dissolved in the HEPES buffer individually. The absorption spectra of dyes showed maximum absorption at 430 nm, and with a shoulder at 590 nm as shown in Fig. 3A. These were added to the Pb^{2+} solutions in a molar ratio of 1:2 (Fig. 3B). However, the visible color change was not observed, except for CA. The optical images of 10 dyes after the addition of various metal ions are provided in (Fig. S1). Based on the screening of absorbance, no single dye formed a complex except CA with Pb^{2+} at 605 nm (Fig. S2). All other dyes were further complexed with other metal solutions as well. The absorption spectra of dye **6** showed that only rhodium metal formed a complex at 510 nm (Fig. S3A), and dye **8** formed complexes with copper at 550 nm (Fig. S3B). None of these complexes showed visible color change and interfered with the CA-Pb^{2+} complex.

Moreover, a mixture of azo dyes was also mixed with various concentrations of CA to evaluate the linearity of CA-Pb^{2+} complex formations in the presence of the other red dyes. The mixture of dyes (Erythrosine B, Acid Red 1, Allura Red AC, and Ponceau 4R) was prepared along with a CA solution of 1 to 90% and the Pb^{2+} solution was prepared in a similar manner. The sample of dyes mixtures without Pb^{2+} was examined and the result showed that all the dyes in the mixture showed maximum absorptions between 450 and 550 nm (Fig. S4A). The lead solution was added to the dye mixture with the same percentage. The result showed that only CA formed a complex with Pb^{2+} at 605 nm. It was observed that the intensity of complex formation increases with an increase in the percentage of CA and Pb^{2+} solution (Fig. S4B).

3.4. Method performance and validation

To find out the detection limit for CA and Pb^{2+} complex in HEPES buffer (pH = 7), a calibration curve was drawn by using the absorbance at 605 nm of the complex versus corresponding concentrations. Two methods were developed without NaF (method I) and with NaF (method II). Linear calibration curves were obtained with excellent correlation coefficients $\geq$ 0.9995 and $\geq$ 0.9901 without and with NaF, respectively. The U.V–visible absorption spectra, calibration curve, and color images of the solution are illustrated (Fig. 4). The limit-of-detection (LOD) and limit-of-quantification (LOQ) were calculated from the regression equation of the standard curve using the standard deviation of the intercept and slope. The LOD and LOQ for the methods I & II were found to be 0.0025 and 0.0076 mg mL^{-1} and 0.0136 and 0.0415 mg mL^{-1}, respectively (Table 2). This indicated excellent sensitivity and selectivity. Intra and inter-day precisions and accuracy of the methods were expressed as %RSD percent relative standard deviation (Table S1). The accuracy was obtained as %bias, while the precision of the method was obtained in terms of %RSD. In all cases, the accuracy of the method was

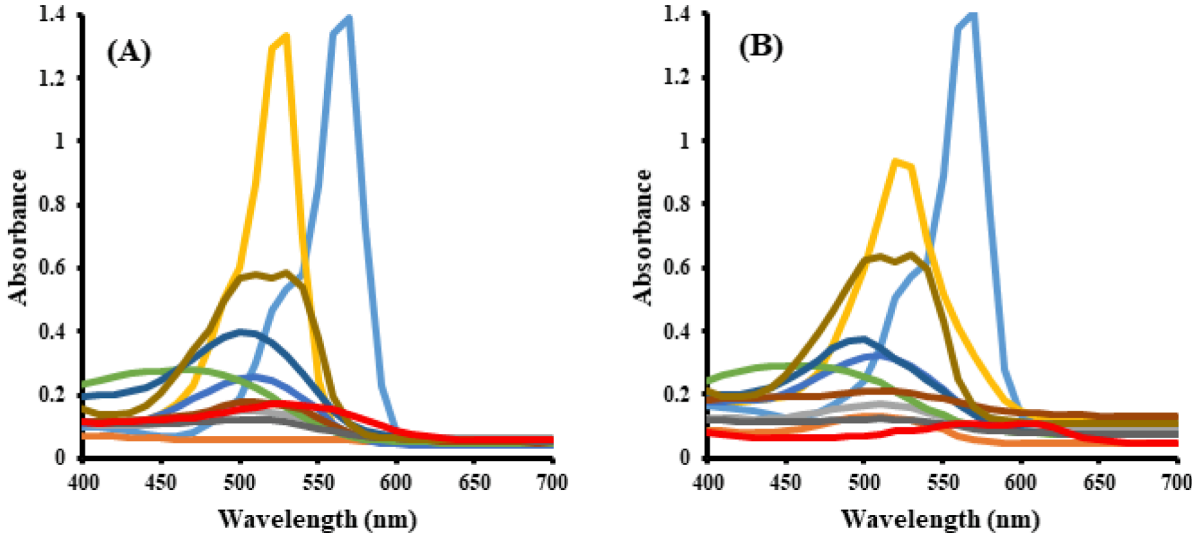

Fig. 3. U.V. visible absorption spectra of dyes (■) CA, (■) Ponceau 4R, (■) Allura Red AC, (■) Carmoisine, (■) Acid Red 1, (■) Amaranth, (■) Erythrosine B, (■) Acid Red 14, (■) Direct Red 17, (■) Ponceau SX, (■) Acid Red 92. (A) Without Pb^{2+} solution. (B) with the presence of Pb^{2+} solution in a mole ratio 1:2.

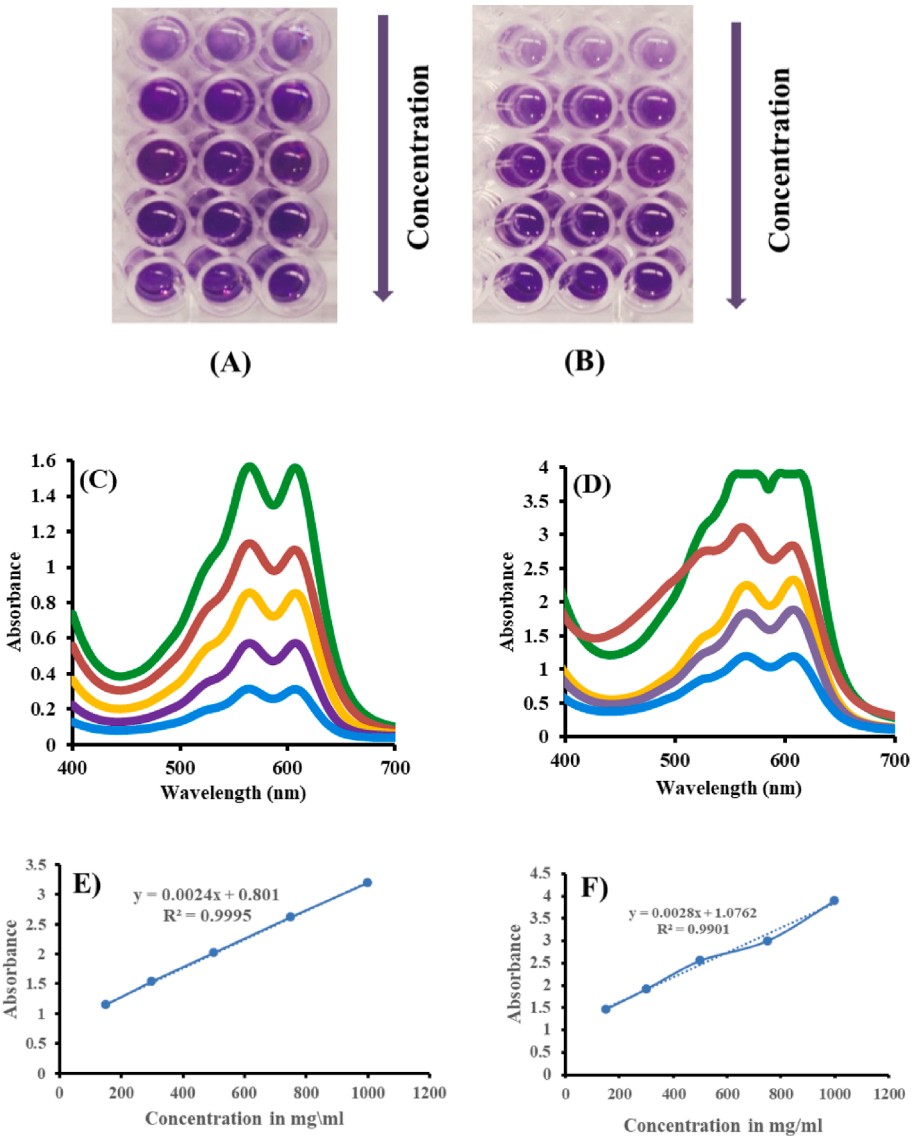

Fig. 4. Image of Calibration solutions of CA-Pb^{2+} complex in triplicates with increasing concentrations of 150–1000 mg/mL (150, 300, 500, 750, 1000 mg/mL) **A)** Without NaF (Method I) and **B)** With NaF (Method II). Calibration curve absorption spectra of CA-Pb^{2+} complex with increasing concentration 150–1000 mg/mL **C)** Without NaF (Method I) and **D)** With NaF (Method II). Calibration curve of CA-Pb^{2+} complex with concentration range 150–1000 mg/mL **E)** without NaF (Method I) and **F)** with NaF (Method II).

found to be > 95% while %RSD was lower than 9%. Method performance was also evaluated through recovery studies in spiked samples. A known amount of CA and Pb^{2+} were used with three concentrations of 0.135, 0.226, and 0.316 mg mL^{-1} for each sample and analyzed by U. V–visible spectrophotometer.

The recovery value was in the range of 95.4 to 128% (on average) (Table S2). The recovery studies were also examined without and with the addition of NaF. As the recovery of the method was not very good with the addition of NaF, this shows that the matrix effect is very high in the sample. Therefore this method was not valid for the quantitative analysis of CA in food and non-food samples.

3.5. Detection of CA in food and non-food samples

CA detection in samples was challenging because the sample matrix can have a significant influence. The extraction procedure is an important factor to ensure that there are no interfering species in food matrices. The absorbance of the extracted CA from samples was recorded, and compared with a standard to confirm the presence of CA. For further verification, the UPLC profile was obtained to analyze the extraction of CA in samples, based on their retention time in comparison to the standard (Fig. S5). In this study, we developed a quick and simple method to detect CA in samples by using lead nitrate as a reagent for direct colorimetric CA detection. The paper strip approach was checked for the selective detection of CA in food and non-food samples. However, the majority of the previously described detection methods relied on instrumental analysis. Therefore, simple and instrument-free detection of CA in food matrices using color visualization was needed. The paper strip was prepared by dipping it in a lead nitrate solution (2 mg mL^{-1}) and drying it. As the prepared paper strip was dipped into the sample, the color change observed within 10 s on the paper strip, as well as the sample solution showed a visible color change from pink to purple due to the CA-Pb^{2+} complex formations (Fig. S6). This paper strip-based method will be further validated for commercial use. However, due to the interference of existing Fe^{2+}/Fe^{3+} in the sample, the color intensity of CA significantly decreased in the sample solution consisting of Fe^{2+}/Fe^{3+}. This suggests that an interference (Fe^{2+} and Fe^{3+}) is due to the complex formation of CA and Fe^{2+} or Fe^{3+}. As a result, false-negative results may appear. For that reason, experiments are also performed to find the interference of Fe^{2+} and Fe^{3+} during the formation of the CA-Pb^{2+} complex. The result of the experiment shows that Fe^{3+} didn't interfere with the formation of the CA-Pb^{2+} complex, but Fe^{2+} interfered with the formation of the CA-Pb^{2+} complex. However, the interference from Fe^{2+} can be reduced by adding 4% NaF (600 μL) as a masking agent. NaF is an effective agent for masking and reducing the interference of Fe^{2+}. The color images of the solution are given in (Fig. S7A & B)

Table 1
Comparison of the previously reported methods of carmine/ CA detection in samples.

S. No	Samples	Method	Method validation				Recovery (%)	Reference
			LOD	LOQ	LR	RSD (%)		
1	Food samples	UHPLC-Q/ Orbitrap MS	0.00 mg kg^{-1}	0.01 mg kg^{-1}	0.01–10 mg kg^{-1}	4.80–5.20	–	[34]
2	Fresh meat/meat products	HPLC-UV-DAD	33.8 ± 2.2 mg kg^{-1}	7.8 mg kg^{-1}	–	–	96.40–8.20	[35]
3	Food samples	Spectrophotometry	0.40 µg L^{-1}	–	1.50–350 µg L^{-1}	3.70	94.80–104.7	[23]
4	Lipstick products	RP-HPLC-PDA	6.42 ng mL^{-1}	21.78 ng mL^{-1}	1.00 ng mL^{-1}	1.25	80–90	[36]
5	Candies	U.V/ Surface-enhanced Raman scattering	0.25 µg mL^{-1}	0.5 µg mL^{-1}	0.50–100 µg mL^{-1}	–	–	[10]
6	Saffron samples	FT-IR/ UV–Visible/ RP-HPLC-DAD	0.03 µg mL^{-1}	0.10 µg mL^{-1}	0.01–5.00 µg mL^{-1}	2.80–6.80	96–101	[37]
7	Meat products	IC-ELISA	1 mg kg^{-1}	0.05 mg kg^{-1}	–	–	79.1–103.1	[38]
8	Vitamin samples	RP-HPLC-DAD	2.40 µg mL^{-1}	7.99 µg mL^{-1}	–	2.42	–	[39]
9	Foodstuffs	Spectrophotometry/ Cloud Point Extraction	0.012 mg L^{-1}	0.04 mg L^{-1}	0.04–5.00 mg L^{-1}	4.80	100.00	[40]
10	Wine and Soft drink	UFLC–MS/MS	1.00 µg L^{-1}	3.33 µg L^{-1}	5.00–1000 µg L^{-1}	1.90–4.60	88–96.60	[41]
11	Candy and milk	Differential pulse polarography	0.18 mg L^{-1}	0.16 mg L^{-1}	1.1–100.5 mg L^{-1}	7.00	95.00	[8]
12	Different samples (food, meat, chol, veg)	HPLC	0.40 µg mL^{-1}	1.00 µg mL^{-1}	1.00–100 µg mL^{-1}	2.80–6.80	90–96	[12]
13	Soft drink	HPLC/ ESI-MS/MS	0.003 mg L^{-1}	–	0.01–0.50 mg L^{-1}	6.10	92.10	[42]
14	Ice cream and soft drinks	Square-wave adsorptive stripping voltammetry	0.01 mg L^{-1}	–	0.05–0.14 mg L^{-1}	2.20	97.20	[15]
15	Different food and non-food samples (color beverages, jellies, candies, lipstick etc)	Spectrophotometry	a) 0.0025 mg mL^{-1} b) 0.0136 mg mL^{-1}	a) 0.0076 mg mL^{-1} b) 0.0415 mg mL^{-1}	a) 0.073–0.492 mg mL^{-1} b) 0.031–0.207 mg mL^{-1}	a) 0.1–2.70 b) 0.0–9.90	a) 95–99.3 b) 107–128	The current method

[a]Without NaF (Method I).
[b]With NaF (Method II).

Table 2
Summary of calibration curve of CA-Pb^{2+} complex, limit-of-detection (LOD), and limit of quantification (LOQ) for the optimized method.

Wavelength (λ_{nm})	Linear calibration range (mg mL^{-1})	Regression equation	R^2	LOD (mg mL^{-1})	LOQ (mg mL^{-1})
605	a) 0.073–0.492	y = 0.0024x + 0.801	0.9995	0.0025	0.0076
605	b) 0.031–0.207	y = 0.0028x + 1.0762	0.9901	0.0136	0.0415

[a]Without NaF (Method I).
[b]With NaF (Method II).

and U.V–visible absorption spectra are provided in (Fig. S8A & B). After the addition of NaF, the sample solution was maintained at pH = 7 by using 1 M NaOH solution. Then the lead solution was added to the sample, and absorbance was recorded.

Several analytical methods have been reported to identify CA using different analytical techniques. However, simple and cost-effective detection of CA in various food and non-food matrices using color visualization is described by us. A comparison of the different reported methods with the current method is presented in Table 1. Our method is based on the complex formation, which shows a clear and visible color change in the presence of CA. This is therefore, a chemosensing approach for the rapid detection of CA.

3.6. *Characterization of CA-Pb^{2+} complex*

The complexation of CA with Pb^{2+} was previously reported with the CA to Pb^{+2} ratio of 1:2 [9]. In our case, a similar result was obtained from the Jobs plot. The Jobs method was implemented by maintaining the concentration of CA and Pb^{2+} at 0.0207 mg mL^{-1}, followed by the continuous variations in the molar ratio of CA and Pb^{2+}. During the experiment, the absorbance was recorded at each point of the mole ratio, and the maximum absorption was reached when the molar fraction of CA was close to 0.35 (Fig. S9). Based on the Jobs plot, the binding stoichiometry was thus evaluated as 1:2 between CA and Pb^{2+}.

A comparison of the IR spectra of the CA-Pb^{2+} complex and CA helped to reveal a few significant differences due to the coordination of Pb^{2+} with CA (Table S3). In the FT-IR spectrum of CA, a characteristic peak at 1705 cm^{-1} corresponded to the carboxylic functionality, which disappeared due to the coordination of the hydroxyl group of carboxylate with the Pb^{2+} ion (Fig. S10). The peaks for the C = O and C = C stretching's was CA at 1608 and 1567 cm^{-1} changed to broad bands in the complex which indicates the participation of the oxygen of the carbonyl groups in metal binding. The peaks between 1428 and 1000 cm^{-1} corresponded to the stretching and bending vibrations of the C–C,

C-OH, and C–H bonds of CA [32] which appeared in different shapes in the CA-Pb^{2+} complex. Moreover, the absorption peak at 722 cm^{-1} due to the Pb–O bond in the complex, was not present in CA. The IR data provided key information about Pb^{2+} binding to CA, based on the perturbation of IR peaks of different functional groups, after the metal complexation of CA.

Based on the mass spectrum, it was inferred that the ratio of CA to Pb^{2+} in the complexes was either 1:1 or 2:1. Since there was no crystal formation in the complex, information obtained from the mass spectrum was crucial. The pseudo molecular ion of CA was at m/z = 493.38 (Fig. S11), while the complexes of CA-Pb^{2+} produced ions at m/z = 699.8 and 1191.2 which correspond to the 1:1 and 2:1 CA-Pb^{2+} complexes of CA with Pb^{2+}, respectively (Fig. S12). As suggested by the Jobs plot, the CA-Pb^{2+} complex in the ratio of 1:2 was not observed in the mass spectrum which could be attributed to its instability in the ESI-MS gas phase.

To establish the correct structure of the CA-Pb^{2+} complexes, the ^{1}H NMR spectra were recorded (Fig. S13 A & B). For instance, the chemical shift of 1-OH in CA at δ 14.59 invariably appeared slightly downfield (Table S4). This indicated the interaction of CA with Pb^{2+} *via* the proton of 1-OH by coordination through an oxygen atom. On the other hand, the signals of the hydroxyl group of carboxylic acid that was indicated to be involved in the coordination with the Pb^{2+} ion did not appear in the ^{1}H NMR spectrum due to the fast exchangeable proton, whereas the protons of other hydroxyl groups remained intact after complexation. The rest of the signals of the complex were slightly shifted as compared to CA due to the conjugation effect between CA and Pb^{2+}.

The spectroscopic data suggested that different CA-Pb^{2+} complexes could exist in the solution in different ratios. This also proposed the structures of CA-Pb^{2+} complexes (Fig. S14) in different ratios. Therefore, the stability of different complexes between Pb^{2+} ions and CA was studied using the density functional theory method. The interaction energies of the different complexes are presented in Table S4. In the case of the 1:1 complex the OH-1 is involved in chelation with a metal ion, and the carbonyl group of the quinone ring was estimated to be the most stable as deduced from the energy value as compared to the other two possible 1:1 CA-Pb^{2+} complexes. The stability of the 2:1 CA-Pb^{2+} complex was evaluated in terms of interaction energy. Based on the coordination mode, two forms, i.e. *cis* and *trans* complexes, were suggested, in which the *trans*-isomer was found to be slightly more stable than the *cis*-isomer. Afterward, the interaction energies were calculated for the 1:2 CA-Pb^{2+} complex as deduced by the Jobs plot, and three possible structures were proposed (Table S5). Among them, the CA-Pb^{2+} complex in which the metal ions were coordinated to the carboxylic acid group and OH-3, and carbonyl of quinone ring and OH-8, was found to be the most stable as compared to the other two 1:2 complexes. It was significant that the stability of these three complexes was obtained after including the solvent effect as the water in the polarizable continuum solvent (PCM) model stabilized the complexes. Interestingly the corresponding complexes were not obtained from the DFT calculations in the gas phase.

An overall structure elucidation of the CA-Pb^{2+} complexes in different ratios revealed that the coordination mode of Pb^{2+} ion to CA varies in the solution but the stability of the complexes is governed by the conformation of the CA which encompasses all possible positions of the molecule and thus help to chelate the metal ion in different ratios. Comparing the geometric configuration of the 1:2 CA-Pb^{2+} complexes, as suggested by the Jobs plot, the relative stability of the complexes was explained by examining their geometric configuration. Fig. 5 illustrates the optimized structure of the CA-Pb^{2+} complexes **A** and **B** in which the coordination modes of the metal ions were shown. The complex **B** was expected to be more stable than complex **A** as the ^{1}H NMR spectrum of the CA-Pb^{2+} complex showed the change in the chemical shift of OH-1 when compared to the spectrum of the CA. Looking at the DFT-optimized structure it can be seen that the metal ion near the OH-1 was out of the plane of the ring, thus indicating the lower stability of complex **A**. On the other hand, complex **B** having the metal ions was coordinated by the OH-5 and carboxylate group, and both the metal ions, in particular the one near the OH-5 were co-linear with the coordinating –OH group along with the carbonyl group of quinone. Moreover, the coordination distance between the two –OH groups (OH-1 and OH-5) and the Pb^{2+} ion was different, as the distance between OH-1 and Pb^{2+} in complex **A** was larger than that of OH-5 with Pb^{2+} in complex **B**. This difference was due to the size of the Pb^{2+} ion which was too large to be accommodated between the ligand groups in complex **B** along with the Pb^{2+} ion that was already coordinated by the carboxylate group. This resulted in the out-of-plane arrangement of the Pb^{2+} ion near OH-1. On the other hand, the metal ion, for instance, Al^{3+} of the same group was reported to be chelated by different functional groups of CA, including OH-1 [33]. However, the 2:1 CA-Al^{3+} and 1:2 CA-Al^{3+} complexes were proposed to OH-5 coordinated with the Al^{+3} ion. Therefore, in the case of Pb^{2+}, it was established by the DFT calculation that the coordination of the OH-5 group with Pb^{2+} produced stable CA-Pb^{2+} complexes.

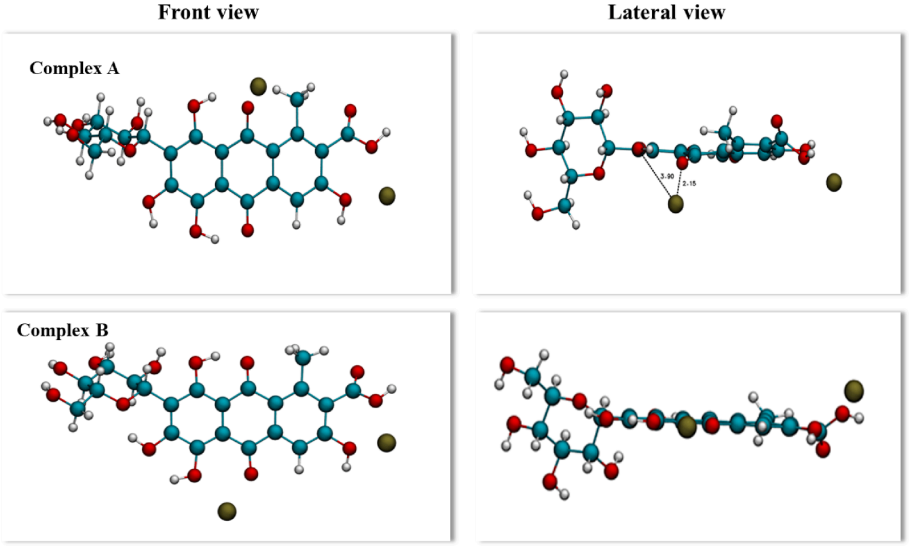

Fig. 5. DFT-optimized structure of 1:2 CA-Pb^{2+} complexed **(A)** and **(B)**.

4. Conclusion

The method reported here is cost-effective and reliable for the qualitative detection of carminic acid (CA) in various food and non-food samples. The CA detection is based on the complexation of CA with Pb^{2+} by visible color change instead of using sophisticated scientific instruments. Furthermore, spectral characterization and DFT calculations have suggested the complexation of CA with Pb^{2+} with a stoichiometry ratio of 1:2. Moreover, the CA-Pb^{2+} complex was formed at neutral pH; therefore, it has broad applications in different fields, such as food, cosmetics, and pharmaceuticals.

CRediT authorship contribution statement

Azra Akbar: Formal analysis, Data curation, Methodology, Visualization, Writing – original draft. **Amna Jabbar Siddiqui:** Investigation, Validation, Visualization, Writing – review & editing. **Syed Tarique Moin:** Data curation, Validation, Writing – review & editing. **Muhammad Noman Khan:** Data curation, Validation, Writing – review & editing. **Ali Raza:** Methodology. **Adeeba Khadim:** Data curation, Visualization, Writing – review & editing. **Muhammad Usman:** Writing – review & editing. **M. Iqbal Choudhary:** Resources, Writing – review & editing. **Syed Ghulam Musharraf:** Supervision, Conceptualization, Writing – review & editing.

Declaration of Competing Interest

The authors declare that they have no known competing financial interests or personal relationships that could have appeared to influence the work reported in this paper.

Data availability

Data will be made available on request.

Acknowledgment

The authors acknowledge the financial support from the Higher Education Commission, Pakistan, under the Center of Excellence (CoE-75) funding program.

Appendix A. Supplementary material

Supplementary data to this article can be found online at https://doi.org/10.1016/j.saa.2023.122953.

References

[1] A. Gürses, M. Açıkyıldız, K. Güneş, M.S. Gürses, Historical development of colorants, in: Dyes and Pigments, Springer, 2016, 1-12.
[2] S. Adeel, F.-U. Rehman, S. Rafi, K.M. Zia, M. Zuber, Environmentally friendly plant-based natural dyes: extraction methodology and applications, in: Plant and Human Health, Volume 2, Springer, 2019, 383-415.
[3] N. Amin, F.-U. Rehman, S. Adeel, T. Ahamd, M. Muneer, A. Haji, Sustainable application of cochineal-based anthraquinone dye for the coloration of bio-mordanted silk fabric, Environ. Sci. Pollut. Res. 27 (2020) 6851–6860.
[4] J. Méndez, M. González, M.G. Lobo, A. Carnero, Color quality of pigments in cochineals (Dactylopius coccus Costa). Geographical origin characterization using multivariate statistical analysis, J. Agric. Food Chem. 52 (2004) 1331–1337.
[5] E. Watson, An alternative to crushed bugs? Chr. Hansen explores producing carmine via controlled fermentation process, FOODnavigator-usa. com, in, 2013.
[6] S. Secinaro, D. Calandra, Halal food: structured literature review and research agenda, Br. Food J. 123 (2021) 225–243.
[7] J. Wang, Z. Wang, J. Liu, H. Li, Q.X. Li, J. Li, T. Xu, Nanocolloidal gold-based immuno-dip strip assay for rapid detection of Sudan red I in food samples, Food Chem. 136 (2013) 1478–1483.
[8] U.T. Yilmaz, F. Ergun, H. Yilmaz, Determination of the food dye carmine in milk and candy products by differential pulse polarography, J. Food Drug Anal. 22 (2014) 329–335.
[9] F. Samari, B. Hemmateenejad, M. Shamsipur, Spectrophotometric determination of carminic acid in human plasma and fruit juices by second order calibration of the absorbance spectra–pH data matrices coupled with standard addition method, Anal. Chim. Acta 667 (2010) 49–56.
[10] C. Garrido, E. Clavijo, S. Copaja, J. Gómez-Jeria, M. Campos-Vallette, Vibrational and electronic spectroscopic detection and quantification of carminic acid in candies, Food Chem. 283 (2019) 164–169.
[11] M. González, J. Méndez, A. Carnero, M.G. Lobo, A. Afonso, Optimizing conditions for the extraction of pigments in cochineals (Dactylopius coccus Costa) using response surface methodology, J. Agric. Food Chem. 50 (2002) 6968–6974.
[12] H. Lim, J. Kim, K. Ko, M. Kim, Determination of hexamethylenetetramine in foods by high-performance liquid chromatography (HPLC), Food Additives & Contaminants: Part A 31 (2014) 1489–1495.
[13] M. Masár, J. Hradski, E. Vargová, A. Miškovčíková, P. Božek, J. Ševčík, R. Szucs, Determination of carminic acid in foodstuffs and pharmaceuticals by microchip electrophoresis with photometric detection, Separations 7 (2020) 72.
[14] M. Puchalska, M. Orlińska, M.A. Ackacha, K. Połeć-Pawlak, M. Jarosz, Identification of anthraquinone coloring matters in natural red dyes by electrospray mass spectrometry coupled to capillary electrophoresis, J. Mass Spectrom. 38 (2003) 1252–1258.
[15] A.H. Alghamdi, H.M. Alshammery, M.A. Abdalla, A.F. Alghamdi, Determination of carmine food dye (E120) in foodstuffs by stripping voltammetry, J. AOAC Int. 92 (2009) 1454–1459.
[16] M. Alizadeh, E. Demir, N. Aydogdu, N. Zare, F. Karimi, S.M. Kandomal, H. Rokni, Y. Ghasemi, Recent advantages in electrochemical monitoring for the analysis of amaranth and carminic acid food colors, Food Chem. Toxicol. 112929 (2022).
[17] M. Soylak, Y.E. Unsal, E. Yilmaz, M. Tuzen, Determination of rhodamine B in soft drink, waste water and lipstick samples after solid phase extraction, Food Chem. Toxicol. 49 (2011) 1796–1799.
[18] M. Herrero, A. Cifuentes, E. Ibañez, Sub-and supercritical fluid extraction of functional ingredients from different natural sources: Plants, food-by-products, algae and microalgae: A review, Food Chem. 98 (2006) 136–148.
[19] P. Qi, T. Zeng, Z. Wen, X. Liang, X. Zhang, Interference-free simultaneous determination of Sudan dyes in chili foods using solid phase extraction coupled with HPLC–DAD, Food Chem. 125 (2011) 1462–1467.
[20] K. Zaghdoudi, S. Pontvianne, X. Framboisier, M. Achard, R. Kudaibergenova, M. Ayadi-Trabelsi, J. Kalthoum-Cherif, R. Vanderesse, C. Frochot, Y. Guiavarc'h, Accelerated solvent extraction of carotenoids from: Tunisian Kaki (Diospyros kaki L.), peach (Prunus persica L.) and apricot (Prunus armeniaca L.), Food Chemistry, 184 (2015) 131-139.
[21] N. Altunay, R. Gürkan, U. Orhan, A new ultrasonic-assisted cloud-point-extraction procedure for pre-concentration and determination of ultra-trace levels of copper in selected beverages and foods by flame atomic absorption spectrometry, Food Addit. Contam. Part A 32 (2015) 1475–1487.
[22] R. Gürkan, S. Korkmaz, N. Altunay, Preconcentration and determination of vanadium and molybdenum in milk, vegetables and foodstuffs by ultrasonic-thermostatic-assisted cloud point extraction coupled to flame atomic absorption spectrometry, Talanta 155 (2016) 38–46.
[23] E. Adil, Interference-free determination of carmine in food samples using ultrasonic assisted cloud point extraction coupled with spectrophotometry, Cumhuriyet Sci. J. 40 (2019) 305–316.
[24] W.R. Wadt, P.J. Hay, Ab initio effective core potentials for molecular calculations Potentials for main group elements Na to Bi, J. Chem. Phys. 82 (1985) 284–298.
[25] W.J. Hehre, R. Ditchfield, J.A. Pople, Self—consistent molecular orbital methods. XII. Further extensions of Gaussian—type basis sets for use in molecular orbital studies of organic molecules, J. Chem. Phys. 56 (1972) 2257–2261.
[26] P.C. Hariharan, J.A. Pople, The influence of polarization functions on molecular orbital hydrogenation energies, Theor. Chim. Acta 28 (1973) 213–222.
[27] R. Ditchfield, W.J. Hehre, J.A. Pople, Self-consistent molecular-orbital methods. IX. An extended Gaussian-type basis for molecular-orbital studies of organic molecules, J. Chem. Phys. 54 (1971) 724–728.
[28] R.A. Gaussian09, 1, mj frisch, gw trucks, hb schlegel, ge scuseria, ma robb, jr cheeseman, g. Scalmani, v. Barone, b. Mennucci, ga petersson et al., gaussian, Inc., Wallingford CT, 121 (2009) 150-166.
[29] M. Trojanowicz, J. Orska-Gawryś, I. Surowiec, B. Szostek, K. Urbaniak-Walczak, J. Kehl, M. Wróbel, Chromatographic investigation of dyes extracted from Coptic textiles from the National Museum in Warsaw, Stud. Conserv. 49 (2004) 115–130.
[30] P. Das, C.K. Jain, S. Roychoudhury, H.K. Majumder, S. Das, Design, synthesis and in vitro anticancer activity of a Cu (II) complex of carminic acid: a novel small molecule inhibitor of human DNA topoisomerase I and topoisomerase II, ChemistrySelect 1 (2016) 6623–6631.
[31] H. Filik, E. Tütem, R. Apak, E. Erçağ, Spectrophotometric determination of gallium (III) with carminic acid and hexadecylpyridinium chloride, Microchim. Acta 129 (1998) 57–63.
[32] F. Gosetti, U. Chiuminatto, E. Mazzucco, R. Mastroianni, E. Marengo, Ultra-high-performance liquid chromatography/tandem high-resolution mass spectrometry analysis of sixteen red beverages containing carminic acid: Identification of degradation products by using principal component analysis/discriminant analysis, Food Chem. 167 (2015) 454–462.
[33] M. Harris, B.K. Stein, J.H. Tyman, C.M. Williams, The structure of the colourant/pigment, carmine derived from carminic acid, J. Chem. Res. 2009 (2009) 407–409.
[34] W. Wu, S. Liu, T. Guo, X. Han, B. Xia, Y. Wan, Q. Han, Y. Zhou, Rapid screening of 70 colorants in dyeable foods by using ultra-high-performance liquid chromatography–hybrid quadrupole–Orbitrap mass spectrometry with customized accurate-mass database and mass spectral library, Food Chem. 356 (2021), 129643.
[35] M. Iammarino, A. Mentana, D. Centonze, C. Palermo, M. Mangiacotti, A. E. Chiaravalle, Dye use in fresh meat preparations and meat products: a survey by a

validated method based on HPLC-UV-diode array detection as a contribution to risk assessment, Int. J. Food Sci. Technol. 55 (2020) 1126–1135.
[36] R. Nevitasar, A. Rohman, S. Martono, Validation and quantitative analysis of carmine and rhodamine b in lipstick formulation, Int. J. App. Pharmaceut 11 (2019) 176–180.
[37] S.A. Ordoudi, C. Staikidou, A. Kyriakoudi, M.Z. Tsimidou, A stepwise approach for the detection of carminic acid in saffron with regard to religious food certification, Food Chem. 267 (2018) 410–419.
[38] F. Yang, H. Wang, J. Yang, Y. Yue, M. Ke, H. Li, D. Wan, F. He, An indirect competitive immunoassay for analysis of carminic acid in meat products, Food Anal. Methods 10 (2017) 3687–3693.
[39] M. Šuleková, A. Hudák, M. Smrčová, The determination of food dyes in vitamins by RP-HPLC, Molecules 21 (2016) 1368.
[40] R. Heydari, M. Hosseini, S. Zarabi, A simple method for determination of carmine in food samples based on cloud point extraction and spectrophotometric detection, Spectrochim. Acta A Mol. Biomol. Spectrosc. 150 (2015) 786–791.
[41] X.-H. Chen, Y.-G. Zhao, H.-Y. Shen, L.-X. Zhou, S.-D. Pan, M.-C. Jin, Fast determination of seven synthetic pigments from wine and soft drinks using magnetic dispersive solid-phase extraction followed by liquid chromatography–tandem mass spectrometry, J. Chromatogr. A 1346 (2014) 123–128.
[42] F. Feng, Y. Zhao, W. Yong, L. Sun, G. Jiang, X. Chu, Highly sensitive and accurate screening of 40 dyes in soft drinks by liquid chromatography–electrospray tandem mass spectrometry, J. Chromatogr. B 879 (2011) 1813–1818.